IL NUOVO CIMENTO **38 C** (2015) 128
DOI 10.1393/ncc/i2015-15128-8

Colloquia: LaThuile15

Latest B-physics results from ATLAS

J. Kirk on behalf of the ATLAS Collaboration

Rutherford Appleton Laboratory - Harwell, UK

received 2 October 2015

Summary. — Recent B-physics measurements from the ATLAS detector at the LHC are presented using data collected during 2011 and 2012. Charmonium production cross-sections are measured and compared to theoretical predictions. First measurements of the production of J/ψ mesons in association with vector bosons are presented. The first observation of an excited B_c meson and a search for the X_b are also reported.

PACS 13.20.Gd – Decays of J/ψ, and other quarkonia.
PACS 13.25.Hw – Decays of bottom mesons.
PACS 14.40.Pq – Heavy quarkonia.

1. – Introduction

The ATLAS detector [1] at the Large Hadron Collider (LHC) is designed as a general purpose detector with the main focus on high transverse momentum (p_{T}) discovery physics. However, it also has a dedicated B-physics programme, the latest results from which are presented here. The B-physics programme concentrates on low p_{T} dimuon B signatures which can be efficiently triggered at an affordable event rate. This allows the study of quarkonia production (an important test of QCD), b-hadrons decaying to $J/\psi X$ (to search for new states and for mixing and CP violation studies) and the search for rare decays of b-hadrons into final states containing two muons.

The most important elements of the ATLAS detector for B-physics measurements are the Inner Detector tracker and the Muon Spectrometer. The Inner Detector covers $|\eta| < 2.5$; it consists of silicon pixel and microstrip detectors and a transition radiation tracker all immersed in a 2 T magnetic field. The Muon Spectrometer consists of precision tracking chambers ($|\eta| < 2.7$) and detectors designed for triggering ($|\eta| < 2.4$) which are within a toroidal magnetic field of about 0.5 T. During 2011 and 2012, ATLAS recorded $5.1\,\mathrm{fb}^{-1}$ and $21.3\,\mathrm{fb}^{-1}$ of data from p-p collisions at centre-of-mass energies of $\sqrt{s} = 7\,\mathrm{TeV}$ and $\sqrt{s} = 8\,\mathrm{TeV}$ respectively.

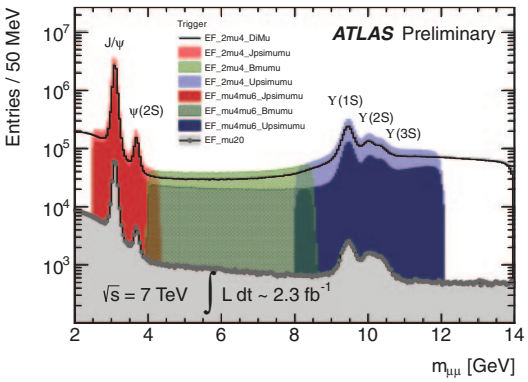

Fig. 1. – Invariant mass of oppositely charged muon candidate pairs selected by a variety of ATLAS triggers. The coloured histograms show those events selected by the dedicated B-physics triggers compared to those triggered by the single muon trigger (grey). The different colours correspond to triggers with different mass ranges (red: 2.5–4.3 GeV ("Jpsimumu"), green: 4–8.5 GeV ("Bmumu"), blue: 8–12 GeV ("Upsimumu").

During low luminosity data-taking in early 2010, B-physics events could be triggered using low momentum single muons. With increasing luminosity, these triggers were either prescaled or had increased thresholds applied which severely limit the acceptance for B-physics events. For this reason, dedicated B-physics triggers based on di-muons had been developed. These require two low momentum muons ($p_{\mathrm{T}} > 4\,\mathrm{GeV}$) to be identified at the first (hardware) level of the trigger. Once the muons are confirmed in the High Level Trigger, a fit is performed to the combined vertex and mass constraints are applied. Figure 1 shows the dimuon mass spectrum for events recorded during the first half of 2011 data taking. The coloured histograms show the significant data sample collected by the dedicated B-physics triggers.

2. – Quarkonium production

Heavy quark production has been studied since the discovery of the J/ψ and Υ in the 1970s but is still not fully understood. The LHC provides the opportunity to test existing models of Quantum Chromo-Dymanics (QCD) in a higher energy regime, higher transverse momentum scale and wider rapidity range than previously.

ATLAS has previously reported production measurements for J/ψ and Υ [2,3]. Here, recent results for the production of $\chi_{c1,2} \to J/\psi\gamma$ [4] and $\psi(2S) \to J/\psi\pi^+\pi^-$ [5] mesons are presented. These charmonium resonances can be produced either promptly in p-p collisions or in non-prompt decays of b-hadrons. The prompt and non-prompt contributions to the cross-section can be resolved by exploiting the displaced vertex of the charmonium arising from B-hadron decays. The pseudo-proper decay time (τ), which uses the mass and transverse momentum of the J/ψ rather than those of the B-hadron, is used as a discriminant:

$$\tau = \frac{L_{xy}\, m_{\mathrm{PDG}}^{J/\psi}}{p_{\mathrm{T}}^{J/\psi}}, \tag{1}$$

where L_{xy} is the transverse decay length of the J/ψ vertex.

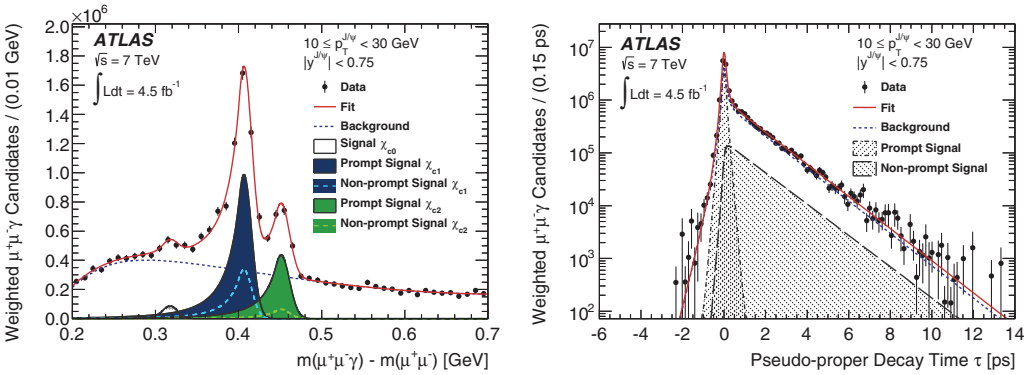

Fig. 2. – Left: The mass difference $\Delta m = m(\mu^+\mu^-\gamma) - m(\mu^+\mu^-)$ for χ_c candidates reconstructed with $10\,\text{GeV} < p_{\text{T}}^{J/\psi} < 30\,\text{GeV}$. Right: Psuedo-proper decay time distribution for the same sample of χ_c candidates. The result of the simultaneous fit to both distributions is shown by the red line.

The selection of J/ψ events is common to the two measurements: two trigger-matched muons with a p_{T} of more than 4 GeV are fitted to a common vertex which must have a χ^2/ndof less than 15. The individual measurements are discussed in the following sections.

2˙1. $\chi_c \to J/\psi\gamma$ *production.* – χ_c candidates are reconstructed through the decay $\chi_c \to J/\psi\gamma$ where the photons (with typical p_{T} of about 1 GeV) are identified through their conversions in the Inner Detector. The rapidity of the J/ψ is required to satisfy $|y^{J/\psi}| < 0.75$; this ensures that the mass resolution is sufficient to distinguish the individual χ_c states. Figure 2 shows the mass difference, $\Delta m = m(\mu^+\mu^-\gamma) - m(\mu^+\mu^-)$, (left) and pseudo-proper decay time (right) distributions for the χ_c candidates. Peaks in the mass distribution corresponding to χ_{c1} and χ_{c2} states are clearly observed above the background. A two-dimensional unbinned maximum-likelihood fit to the Δm and τ distributions is used to extract the prompt and non-prompt cross-sections. The red line shows the projection of the result of the fit used to extract the prompt and non-prompt fractions.

Figure 3 shows the differential cross-sections for prompt χ_{c1} (left) and non-prompt χ_{c1} and χ_{c2} (right) production as a function of the p_{T} of the J/ψ. These are the first absolute measurements of χ_c production cross-sections. Reference [4] also includes distributions for the prompt χ_{c2} production and cross-section distributions as a function of the p_{T} of the χ_c meson. The prompt cross-sections agree well with the next-to-leading-order (NLO) NRQCD model [6-8]. At leading order, the colour-singlet model [9] (LO CSM) underestimates the production while the k_{T} factorisation model [10, 11] overestimates it. The non-prompt production cross-sections are compared to calculations from the FONLL [12, 13] framework and good agreement between theory and experiment is observed.

For the prompt production a measurement of the ratio of χ_{c1} to χ_{c2} production is made and is shown in fig. 4 (left). The resulting distribution as a function of the p_{T} of the J/ψ is compared to measurements from CMS [14] and to theoretical predictions. The ATLAS and CMS data are consistent and are well described by the NLO NRQCD prediction while the CSM underestimates the ratio. The prompt production cross-section presented here is also combined with the previous ATLAS measurement of the J/ψ cross-

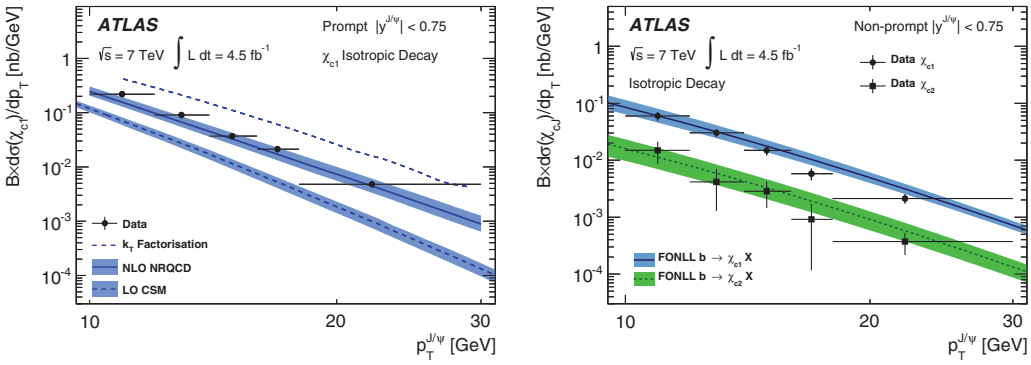

Fig. 3. – Left: Differential cross-sections for prompt χ_{c1} production as a funtion of $p_{\mathrm{T}}^{J/\psi}$. The predictions of NLO NRQCD, the k_{T} factorisation model and the LO CSM are compared to the measurements. Right: Differential cross-sections for non-prompt χ_{c1} and χ_{c2} production as a funtion of $p_{\mathrm{T}}^{J/\psi}$. The predictions of FONLL are compared to the measurements.

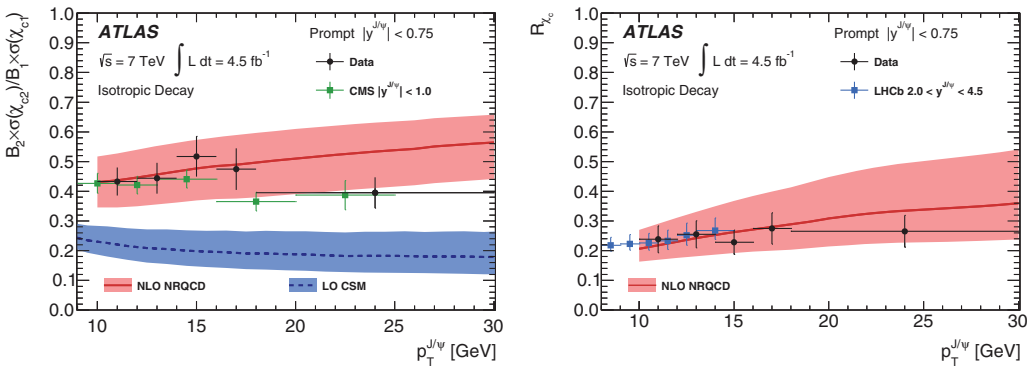

Fig. 4. – Left: The production cross-section of prompt χ_{c2} relative to χ_{c1} measured as a function of $p_{\mathrm{T}}^{J/\psi}$. The measurements are compared to the predictions of NLO NRQCD and the LO CSM. The measurement from CMS [14] is also shown. Right: The fraction, R_{χ_c}, of prompt J/ψ produced in χ_c decays as a function of $p_{\mathrm{T}}^{J/\psi}$. The measurements are compared to the prediction of NLO NRQCD and the measurement from LHCb [15] is also shown.

section [2] to determine the fraction of prompt J/ψ which originate from χ_c feed-down (R_{χ_c}) and this is shown in fig. 4 (right). The measurement agrees well with NLO NRQCD and is compatible with the LHCb data [15] although it should be noted that the rapidity ranges of the two datasets are different.

2˙2. $\psi(2S) \to J/\psi\pi^+\pi^-$ *production.* – The measurement of prompt production of $\psi(2S)$ is a good test of theoretical predictions as it is not affected by any significant feed-down from higher quarkonium states. The $\psi(2S) \to J/\psi\pi^+\pi^-$ candidates are formed by combining J/ψ candidates with two other tracks and performing a four-track vertex fit. This results in an excellent mass resolution of 5.6 MeV. Measurements of prompt and non-prompt cross-sections are compared to theory and other experiments. Figure 5 shows the prompt cross-section compared to theoretical predictions. As with the χ_c measurement, the $\psi(2S)$ cross-section is seen to agree well with the NLO NRQCD prediciton.

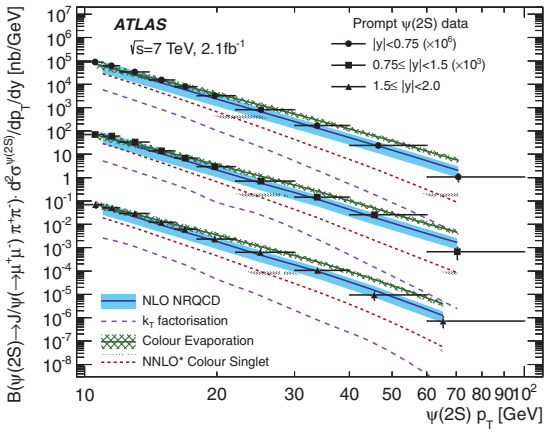

Fig. 5. – Differential cross-sections for prompt $\psi(2S)$ production as a function of $\psi(2S)$ transverse momentum for three rapidity intervals, compared to theoretical predictions.

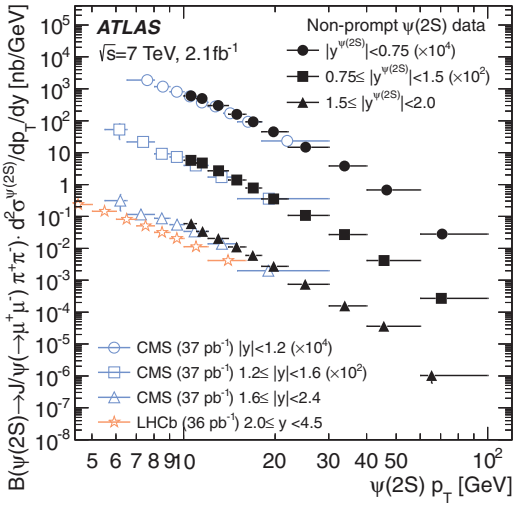

Fig. 6. – Measured differential cross-sections for non-prompt $\psi(2S)$ production as a function of $\psi(2S)$ transverse momentum for three rapidity intervals. Overlaid on the results are measurements from the CMS [16] and LHCb [17] experiments.

In this case, the k_{T} factorisation underestimates the production cross-section and this is correlated to the over-estimate of the χ_c production. Figure 6 shows the non-prompt cross-section compared to measurements from CMS [16] and LHCb [17] in similar or neighbouring rapidity intervals. The ATLAS data extend to higher p_{T} and the data are conisstent where they overlap, again noting that the LHCb data are in a different rapidity region.

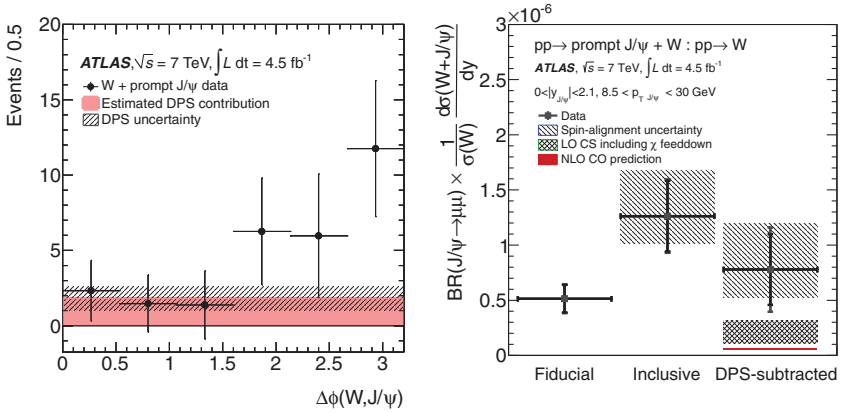

Fig. 7. – Left: $\Delta\phi$ distribution for W + prompt J/ψ events. The DPS contribution is overlaid. Right: The W + prompt J/ψ to W production cross-section ratio in the J/ψ fiducial region, after correction for J/ψ acceptance ("Inclusive") and after subtraction of the DPS component. The LO colour-singlet and NLO colour-octet predictions for SPS and also shown.

3. – Associated production of vector boson with J/ψ

Measurements of associated production of vector bosons with quarkonium states, such as J/ψ, can provide insight into quarkonium production mechanism in a new environment. Two production mechanisms are possible: single parton scattering (SPS) where the two objects are from the same diagram and double parton scattering (DPS) where the two objects are produced from separate hard scatters in the same proton-proton collision. Event by event these processes are indistinguishable but the aim is to find observables which can be used to disentangle them on a statistical basis. One such observable is the azimuthal angle ($\Delta\phi$) between the vector boson and the J/ψ. This angle is expected to be uniform for independent DPS processes but to peak around π for SPS events. Analyses are presented here of W [18] and Z [19] boson production in association with J/ψ.

3˙1. *Prompt J/ψ + W.* – $4.5\,\mathrm{fb}^{-1}$ of data from 2011 is used to select events containing W bosons through combination of a single high p_{T} muon and large missing transverse energy from the neutrino. As in the previous analyses, the J/ψ mass and pseudo-proper decay time distributions are fitted to extract the prompt J/ψ component; 27 signal events are observed with a significance of 5.1σ. This is the first observation of this process. The contribution from DPS is estimated from W+ 2-jet events under the assumption that the W and J/ψ contributions are independent and uncorrelated. Figure 7 (left) shows the $\Delta\phi$ distribution for selected events: it appears to show both DPS and SPS components. The cross-section is measured relative to the inclusive W cross-section. Figure 7 (right) shows the fiducial and inclusive cross-section ratio and the ratio after subtraction of the DPS component. The resulting SPS cross-section ratio is compared to a LO colour-singlet model and NLO colour-octet model [20]. The theoretical predicitions lie below the data but are compatible within 2σ of the experimental uncertainties.

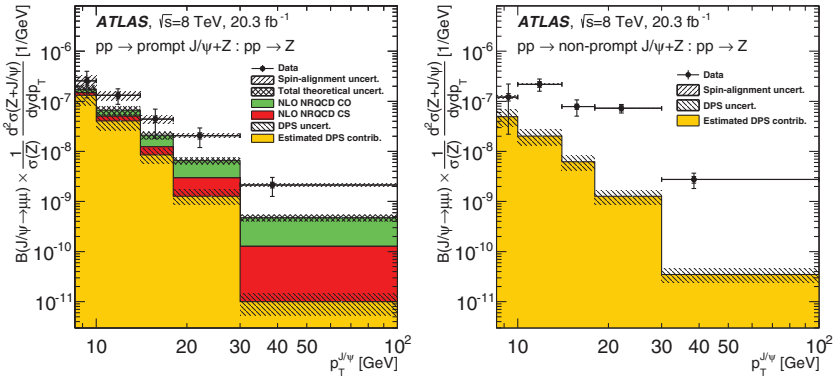

Fig. 8. – Left: Normalised production cross-sections for Z bosons in association with prompt (left) and non-prompt (right) J/ψ as a function of J/ψ transverse momentum. Overlaid on the measurement is the contribution from the total signal originating from DPS interactions. For the prompt production, theoretical predictions at NLO accuracy for the SPS contributions from colour-singlet and colour-octet processes are added to the DPS estimate and are shown as solid bands.

3˙2. J/ψ + Z. – For the $J/\psi + Z$ analysis, similar measurements are performed using $20.3\,\text{fb}^{-1}$ of 2012 data. Z bosons are selected by requiring pairs of oppositely charge electrons or muons with an invariant mass close to the Z mass. The higher statistics used in this analysis means that it is possible to make a measurement for both the prompt and non-prompt J/ψ events. These first measurements of Z boson production in association with prompt and non-prompt J/ψ both have a significance in excess of 5σ. As in the J/ψ + W measurement, a rise in the number of events is observed at high $\Delta\phi$ in both prompt and non-prompt cases. The small $\Delta\phi$ region is sensitive to DPS contributions. By assuming that all observed signal in the first $\Delta\phi$ bin is due to DPS, a limit on the maximum allowed DPS contribution to the observed signal can be determined and this corresponds to a lower limit on σ_{eff} (the effective area parameter regulating multiple-parton interactions). Using the prompt production (where the relative DPS contribution is largest) a lower limit of 5.3 (3.7) mb at 68% (95%) confidence level is placed on σ_{eff}. Normalised differential production cross-sections are determined as a function of J/ψ transverse momentum and are shown in fig. 8.

4. – Observation of excited B_c meson

The spectrum and properties of the B_c meson family are predicted by non-relativistic potential models, perturbative QCD and lattice calculations. The second S-wave state is expected to have a mass in the range 6835–6917 MeV [21], but no excited states of B_c have been observed previously. Here ATLAS reports an observation of the $B_c(2S)$ state in the cascade decay $B_c^{\pm}(2S) \to B_c^{\pm}(1S)\pi^+\pi^-$ with $B_c^{\pm}(1S) \to J/\psi\pi^{\pm}$ [22].

The analysis uses $4.9\,\text{fb}^{-1}$ of 7 TeV and $19.2\,\text{fb}^{-1}$ of 8 TeV data collected during 2011 and 2012, respectively. The analysis is optimised separately at the two centre of mass energies, as the pileup conditions are different in the two cases. $B_c^{\pm}$ candidates are reconstructed using a mass-constrained fit. The fitted $B_c^{\pm}$ mass is consistent with the world average [23] and candidates within a $\pm 3\sigma$ mass window of the fitted mass are combined with two further tracks to reconstruct $B_c^{\pm}(2S)$ candidates. A J/ψ mass constraint is

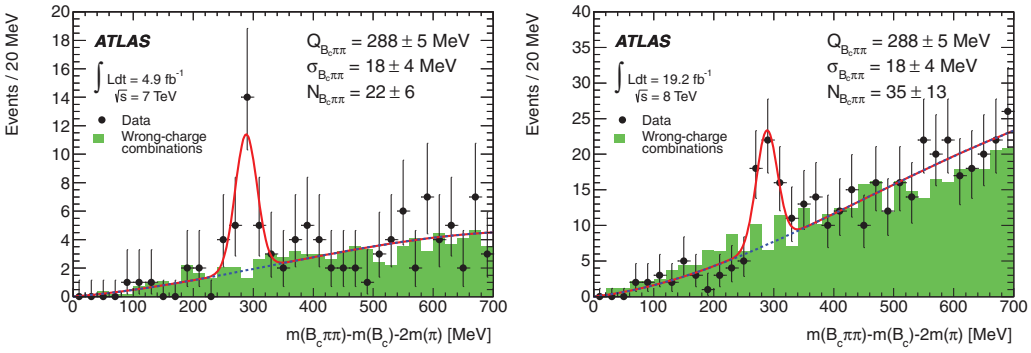

Fig. 9. – Distribution of Q-values for $B_c^{\pm}(2S)$ candidates from 2011 (left) and 2012 (right) data.

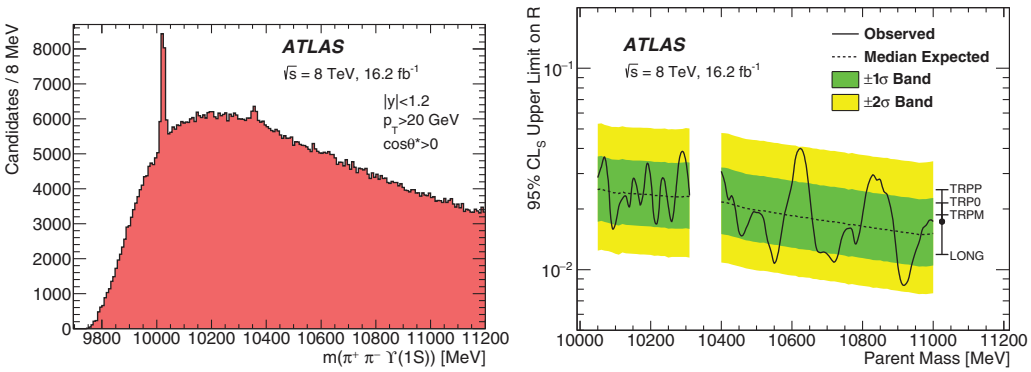

Fig. 10. – Left: The $\pi^+\pi^-\Upsilon(1S)$ mass distribution in the kinematic bin most sensitive to an expected X_b signal: $|\eta| < 1.2$, $p_{\mathrm{T}} > 20\,\mathrm{GeV}$ and $\cos\theta^* > 0$. Right: Observed 95% CL_S upper limits (solid line) on the relative production rate of a hypothetical X_b parent state decaying isotropically to $\pi^+\pi^-\Upsilon(1S)$ as a function of mass. The median expectation (dashed) and the corresponding $\pm1\sigma$ and $\pm2\sigma$ bands (green and yellow, respectively) are also shown. The bar on the right shows typical shifts under alternative X_b spin-alignment scenarios, relative to the isotropic case shown with the solid point.

used and the $B_c^{\pm}$ momentum is required to point to the $B_c^{\pm}(2S)$ vertex. Figure 9 shows the Q-value distribution of $B_c^{\pm}(2S)$ candidates for data taken during 2011 (left) and 2012 (right), where Q is the mass difference given by

$$Q = m(B_c^{\pm}\pi^+\pi^-) - m(B_c^{\pm}) - m(\pi^+\pi^-). \tag{2}$$

There is a clear peak structure observed in the distribution. The Q-value distribution is fitted using a third-order polynomial to model the background and a Gaussian function for the peak structure. The significance of the structure is evaluated using pseudo-experiments and is found to be 3.7σ in the 7 TeV data and 4.5σ in the 8 TeV data; the combined significance is 5.2σ. The error-weighted mean mass is $6842 \pm 4(\mathrm{stat}) \pm 5(\mathrm{syst})\,\mathrm{MeV}$, consistent with the predicted mass of the $B_c^{\pm}(2S)$.

5. – Search for X_b

Heavy quark symmetry would suggest the existence of a state, X_b, which could decay to $\Upsilon\pi^+\pi^-$ in an analogous way to the $X(3872)$ decay to $J/\psi\pi^+\pi^-$. The expected mass of such a state would be about 10.5 GeV. ATLAS has searched for such a state in the $\pi^+\pi^-\Upsilon(1S)$ mass spectrum [24]. Figure 10 (left) shows the observed mass spectrum where the only observed peaks are from the expected $\Upsilon(2S)$ and $\Upsilon(3S)$. Since no signal is observed, upper limits are evaluated at the 95% confidence limit using the CL_s approach. The limits on the product of the X_b cross-section and branching ratio relative to those of the $\Upsilon(2S)$ (R) are shown in fig. 10.

REFERENCES

[1] ATLAS Collaboration, *JINST*, **3** (2008) S08003.
[2] ATLAS Collaboration, *Nucl. Phys. B*, **850** (2011) 387.
[3] ATLAS Collaboration, *Phys. Rev. D*, **87** (2013) 052004.
[4] ATLAS Collaboration, *JHEP*, **07** (2014) 154.
[5] ATLAS Collaboration, *JHEP*, **09** (2014) 079.
[6] Ma Y. Q., Wang K. and Chao K. T., *Phys. Rev. D*, **83** (2011) 111503.
[7] Shao H. S., *Comput. Phys. Commun.*, **184** (2013) 2562.
[8] Ma Y.Q., Wang K. and Chao K. T., *Phys. Rev. Lett.*, **106** (2011) 042002.
[9] Harland-Lang L. A. and Stirling W. J., `http://superchic.hepforge.org/chigen.html`.
[10] Baranov S., Lipatov A. and Zotov N., *Phys. Rev. D*, **85** (2012) 014034.
[11] Baranov S., *Phys. Rev. D*, **83** (2011) 034035.
[12] Cacciari M. *et al.*, *JHEP*, **10** (2012) 137.
[13] Cacciari M., Greco M. and Nason P., *JHEP*, **05** (1998) 007.
[14] CMS Collaboration, *Eur. Phys. J. C*, **72** (2012) 2251.
[15] LHCb Collaboration, *Phys. Lett. B*, **718** (2012) 431.
[16] CMS Collaboration, *JHEP*, **1202** (2012) 011.
[17] LHCb Collaboration, *Eur. Phys. J. C*, **72** (2012) 2100.
[18] ATLAS Collaboration, *JHEP*, **04** (2014) 172.
[19] ATLAS Collaboration, *Accepted by Eur. Phys. J.*, arXiv:1412.6428.
[20] Li G., Song M., Zhang R. Y. and Ma W. G., *Phys Rev D*, **83** (2011) 014001.
[21] Dowdall R. J., Davies C. T. H., Hammant T. C. and Horgan R. R., *Phys. Rev. D*, **86** (2012) 094510.
[22] ATLAS Collaboration, *Phys. Rev. Lett.*, **113** (2014) 212004.
[23] Particle Data Group, *Phys. Rev. D*, **86** (2012) 010001.
[24] ATLAS Collaboration, *Phys. Lett. B*, **740** (2015) 199.